Reversible Refolding of the Diphtheria Toxin T-Domain on Lipid Membranes†

Alexey S. Ladokhin,*,§,‡ Rachel Legmann,⊥ R. John Collier,⊥ and Stephen H. White§

Department of Physiology and Biophysics, University of California, Irvine, California 92697-4560, and Department of Microbiology and Molecular Genetics, Harvard Medical School, Boston, Massachusetts 02115

Received December 1, 2003; Revised Manuscript Received February 1, 2004

ABSTRACT: The catalytic domain of diphtheria toxin (DT) is translocated across endosomal membranes by the T-domain (DTT) in response to acidification. Understanding the energetics of translocation, besides clarifying the mechanism of translocation, should provide insights into general principles of membrane protein stability and assembly. As a first step, we have evaluated the energetics of DTT binding to lipid vesicles using three single-cysteine mutants (L350C, Q369C, and Y280C) labeled with a 7-nitrobenz-2-oxa-1,3-diazol-4-yl (NBD) fluorophore sensitive to polarity changes. Remarkably strong association with the vesicles was detected for all mutants, even at pH 7 at which DTT is believed to be in a fully folded membrane-incompetent state. Lowering the pH in the presence of anionic membranes resulted in a strong but reversible increase in emission of NBD-labeled mutants, consistent with reversible membrane insertion. This reversibility permitted free energies of DTT interactions with vesicles to be determined for the first time. Free energy values for the three mutants ranged from −8 to −10 kcal mol^{-1} at pH 4.3 and from −7 to −8 kcal mol^{-1} at pH 7. Insights into the disposition of DTT on membranes were obtained using a novel hydropathy analysis that considers the relative free energies of transmembrane and interfacial interactions as a function of pH. This analysis suggests that interactions at the membrane interface dominate pH-triggered insertion of DTT, implying that the folding pathway involves interfacial intermediates.

Protein sorting and trafficking across various membranes is a vital function that is generally achieved by complex multiprotein assemblies, such as the mitochondrial TIM and TOM complexes (*1*) and the Sec61 translocon complex of the endoplasmic reticulum (*2*, *3*). Remarkably, many toxic proteins can translocate their water-soluble catalytic domains across membranes without the assistance of these complex machines. In diphtheria, tetanus, and botulinum toxins, translocation occurs in response to acidification of the endosome and is mediated by an α-helical domain situated between an N-terminal catalytic and a C-terminal receptor-binding domain (*4*). In the case of diphtheria toxin (DT), this domain consists of a 10-helix bundle, termed the T-domain (DTT).[1] DTT can also assist the translocation of some heterologous proteins across lipid bilayers (*5*), indicating a general rather than specific translocation pathway. The mechanism of translocation is not understood, but it must involve the refolding of DTT on membranes in response to changes in pH. To begin to understand the mechanism of this process, two questions need to be answered: how does DTT associate with the membrane at neutral pH, and how does it refold and insert at low pH? Most previous studies have focused on the topology of the low-pH inserted state. Here we consider the binding and presumed refolding of DTT on membranes at neutral pH, which is a largely unexplored area. A complete picture of DTT binding, refolding, and insertion should help us to understand the thermodynamic context within which the TIM, TOM, and Sec61 complexes (*1*−*3*) must operate.

The crystallographic structure (*6*) of the water-soluble form of DTT provides a starting point for studying the refolding/insertion process (Figure 1A). Previous studies have disclosed the conformations of transmembrane helical regions (*7*, *8*) and two proposed topologies of the open channel state (*9*). The consensus initial insertion domain consists of the helical hairpin TH8−9 (highlighted in blue in Figure 1A), but the topology of the rest of the structure is less clear (*9*). At low pH, the insertion domain has been shown to exist in two conformations, deep (presumably transmembrane) and shallow (presumably interfacial) (*10*). A recent study of Chenal et al. (*11*) suggested that membrane insertion of DTT consists of several refolding steps with pK_a values ranging from 2.5 to 6.75. This study also presented evidence that both electrostatic and hydrophobic interactions are involved in different stages of insertion, which is often the case for membrane-active peptides (*12*) and larger proteins (*13*, *14*). However, the nature of the membrane-associated state of DTT at neutral pH is unknown, as are the energetics of the membrane insertion process.

† This research was supported by NIH Grants GM-46823 and GM-68002 awarded to S.H.W. by the National Institute of General Medical Sciences and Grant AI-22021 awarded to R.J.C. by the National Institute of Allergy and Infectious Diseases.

* To whom correspondence should be addressed. Phone: 949-824-6993. Fax: 949-824-8540. E-mail: ladokhin@uci.edu.

‡ Permanent address: Institute of Molecular Biology and Genetics, National Academy of Sciences of Ukraine, Kiev 03143, Ukraine.

§ University of California, Irvine.

⊥ Harvard Medical School.

[1] Abbreviations: DTT, diphtheria toxin T-domain; DTT350-NBD, DTT369-NBD, and DTT380-NBD, NBD-labeled single-cysteine mutants L350C, Q369C, and Y380C of DTT, respectively; IANBD amide, *N*,*N*′-dimethyl-*N*-(iodoacetyl)-*N*′-(7-nitrobenz-2-oxa-1,3-diazol-4-yl)-ethylenediamine; LUV, extruded large unilamellar vesicles of 100 nm diameter; NBD, 7-nitrobenz-2-oxa-1,3-diazol-4-yl; POPC, palmitoyloleoylphosphatidylcholine; POPG, palmitoyloleoylphosphatidylglycerol; HΦ, hydrophobic; ES, electrostatic; TM, transmembrane; IF, interfacial.

10.1021/bi036157w CCC: $27.50
Published on Web 05/19/2004

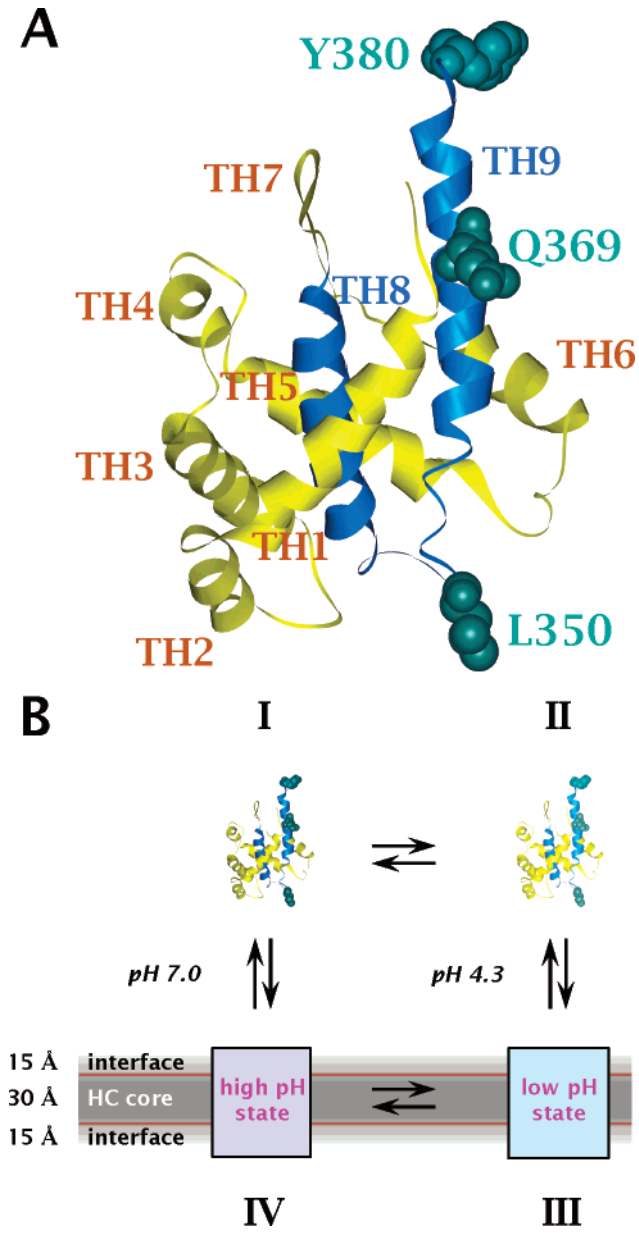

FIGURE 1: The solution structure of (A) diphtheria toxin T-domain (DTT) and (B) a proposed refolding pathway. Panel A shows the crystallographic structure of DTT in water-soluble form (*6*) with the consensus membrane insertion helical hairpin (*9*) highlighted in blue. Three residues, L350, Q369, and Y380 (shown as CPK models), were replaced with cysteine one at a time and labeled with NBD to study membrane association of DTT. Panel B shows the thermodynamic cycle used in the analysis of pH-dependent membrane insertion of DTT (see text for details). The membrane is represented in a manner that distinguishes the hydrocarbon core from an interfacial region (*42*, *43*), suggested to play an important role in refolding of proteins (*32*).

The simplest thermodynamic cycle for describing membrane interactions of DTT consists of four states (Figure 1B). At neutral pH, DTT is a fully folded soluble protein (state I, also known as the S-state) that can be reversibly converted into a molten globule-like state (state II, also known as the A-state) by lowering the pH (*11*). This is a functionally active state, and addition of membranes at low pH results in membrane insertion, translocation of the N-terminus, and ultimately, formation of a pore (state III). Because no translocation or pore-formation has been observed for the addition of DTT to membranes at neutral pH, the existence of state IV (Figure 1B) has been problematic. The data presented here clearly indicate that DTT indeed binds to membranes at pH 7 and higher. Furthermore, we demonstrate for the first time that the transition between the different membrane-bound states of DTT is reversible, which opens the way for a true thermodynamic exploration of spontaneous T-domain insertion. We have consequently been able to obtain the first experimental estimate of the free energy changes of the insertion process using a series of fluorescently labeled single-cysteine mutants of DTT. Computational analyses carried out with experiment-based whole-residue hydrophobicity scales (*15*) indicate the likely importance of an interfacial intermediate state along the DTT membrane insertion pathway.

MATERIALS AND METHODS

Materials. POPC[1] and POPG were purchased from Avanti Polar Lipids (Alabaster, AL). IANBD was purchased from Molecular Probes (Eugene, OR). Two buffers, acidic and neutral, were used in this study. The acidic buffer (pH 4.3) was composed of 10 mM sodium acetate and 50 mM NaCl and the neutral buffer (pH 7.0) of 10 mM HEPES and 50 mM NaCl, unless otherwise indicated. The pH was changed in the course of an experiment by adding appropriate aliquots of a 0.4 M solution of Na_2HPO_4 (to raise pH to 7), 0.5 M solution of NaH_2PO_4 (to lower pH to 5), or a 0.5 M solution of sodium acetate (to lower pH to 4.3).

NBD Labeling of Single-Cysteine Mutants of DTT. Single-cysteine mutations were made at positions L350, Q369, and Y380, and the mutants were isolated as described previously (*16*). NBD labeling was done using a standard procedure for the thiol-reactive derivative IANBD (*17*). In a typical labeling reaction, five 1 μL aliquots of 0.4 M IANBD in DMSO were mixed with 1 mL of a 2 mg/mL sample of a single-cysteine DTT mutant in buffer at pH 7. The sample was incubated overnight at 4 °C in the dark and then passed through a PD-10 gel filtration column to remove IANBD. The extent of labeling was found to be in the range of 0.3−0.8, estimated from absorbance spectra using extinction coefficients of 25 000 M^{-1} cm^{-1} for NBD at 480 nm (*17*) and 17 000 M^{-1} cm^{-1} for DTT at 280 nm.

Vesicle Preparation. Large unilamellar vesicles of diameter 0.1 μm were prepared by extrusion (*18*, *19*) using POPC or a 1:3 molar mixture of POPG and POPC.

Fluorescence. Fluorescence was measured using an SLM 8100 steady-state fluorescence spectrometer (Jobin Yvon, Edison, NJ, former SLM/Aminco, Urbana, IL) equipped with double-grating excitation and single-grating emission monochromators. The measurements were made in 4 mm × 10 mm or 2 mm × 10 mm cuvettes thermostated to 25 °C. Cross-orientation of polarizers was used (excitation polarization set to horizontal, emission polarization set to vertical) to minimize the scattering contribution from vesicles and to eliminate spectral polarization effects in monochromator transmittance (*20*). NBD fluorescence spectra were obtained by averaging 3−20 scans collected over a 480−600 nm range using 1 nm steps. The excitation wavelength was 470 nm. Excitation and emission slits were no larger than 8 nm. The background spectra collected with the same concentration of lipid but without DTT were subtracted from the spectra collected from protein-containing samples. During fluores-

cence kinetics measurements, the entrance slit on the excitation monochromator was reduced to 1 nm to minimize photobleaching. The intensity of control samples of NBD−PE or NBD-labeled DTT remained unchanged for many hours under these conditions. During kinetic measurements, the emission monochromator was set to 530 nm and the slits to 16 nm.

Determination of the Free Energy of Membrane Partitioning. Fluorescence intensities (I) obtained in lipid titration experiments were fitted to (*20*, *21*)

$$I([\mathrm{L}]) = 1 + I_{\infty}\frac{K_x[\mathrm{L}]}{[\mathrm{W}] + K_x[\mathrm{L}]} \quad (1)$$

wherein K_x is the mole-fraction partition coefficient, I_{∞} is the fluorescence increase upon complete binding, [L] is the lipid concentration, and [W] is the concentration of water (55.3 M). Nonlinear least-squares analysis was performed using the Origin 7.0 software package (OriginLab, Inc., Northampton, MA). The free energies of transfer from water to membrane were calculated from the mole-fraction partition coefficients using

$$\Delta G = -RT \ln K_x \quad (2)$$

Hydropathy Calculations. Hydrophobicity (HΦ) profiles were calculated (*22*, *23*) using the Wimley−White scales for interfacial (*15*) and octanol (transmembrane) partitioning (*23*, *24*). The profiles result from a 19-residue sliding-window sum implemented using Membrane Protein Explorer (MPEx), which is available over the World Wide Web from the University of California at Irvine as a Java applet (http://blanco.biomol.uci.edu/mpex). Because these are absolute free energy scales, the zero level distinguishes favorable from unfavorable interactions. The default implementation of MPEx uses free energies computed for transfers from membrane to water. Consequently, any positive point on the HΦ plot represents a favorable transfer free energy for the entire 19-residue sequence centered at that point. The electrostatic (ES) component of free energy of interfacial partitioning was calculated in the following fashion. First, the charge values of 0, 1, and −1 were assigned to each neutral, cationic, and anionic residue in the sequence, respectively. Second, the charge profile was created as a 19-residue sliding-window sum using the same sign convention used in MPEx HΦ profiles. Third, the ΔG profile was generated by multiplying this charge profile by the Faraday constant and the surface potential (*12*). We chose a value of −40 mV for the latter, because it is close to the surface potential in our POPC/POPG experimental system. The HΦ and ES free energies are not strictly additive (*12*), but we nevertheless added the ES ΔG profile to the HΦ profile as a means of obtaining a first-order approximation of the combined ES and HΦ free energies.

RESULTS

Experimental Determination of DTT Free Energy of Transfer. We followed membrane interactions of three single-cysteine mutants of DTT (L350C, Q369C, and Y380C) with POPC/POPG membranes by measuring the fluorescence response of the NBD fluorophore attached to the cysteine residue. The mutants were chosen in such a way that the label was exposed to the aqueous phase on three different sides of the folded protein and have different membrane topologies in the inserted state (Figure 1A). A variety of structural (*7*, *8*, *25*) and functional studies (*9*, *26*−*28*) indicate that the TH8−TH9 helical hairpin (highlighted in blue) inserts across the bilayer at acidic pH in such a way that L350 is translocated across the membrane, Q369 is inserted close to the hydrocarbon core, and Y380 remains untranslocated on the cis side of the bilayer. For all three mutants, NBD fluorescence increased upon the addition of LUV, indicating membrane interactions. Typical kinetic and spectral data are shown in Figure 2 for DTT350-NBD. At pH 7, in the absence of vesicles, fluorescence was rather low and the position of emission maximum was about 533 nm (level 1, Figure 2A). Upon addition of LUV, fluorescence increased and the maximum shifted to 531 nm (level 2). This indicated that interaction with the membrane occurs even at the

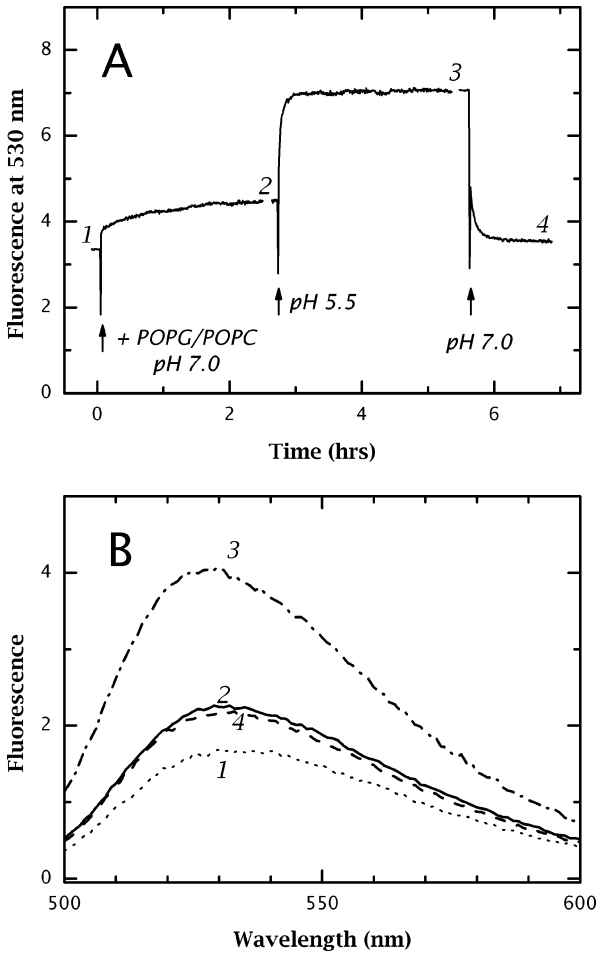

FIGURE 2: Reversibility of pH-triggered membrane insertion of DTT into anionic large unilamellar vesicles (LUV) composed of 1:3 POPG/POPC: (A) fluorescence kinetics of a single sample of the NBD-labeled DTT L350C mutant was measured in buffer and in the presence of anionic membranes under changing conditions of pH; (B) measurements of the NBD emission spectra made after the intensities in panel A had reached equilibrium. These spectra were taken at times corresponding to the labeled positions in panel A and are numbered according to the following progression of changes: (1) 0.3 μM DTT350-NBD in 1 mL of a solution of 10 mM phosphate buffer at pH 7.0; (2) 0.5 mM 75POPC/25POPG LUV added; (3) pH changed to 5.5 by addition of 0.1 mL of 0.5 M monobasic phosphate; (4) pH returned to 7.0 by addition of 0.2 mL of 0.4 M dibasic phosphate. All spectra (but not the kinetic traces) are corrected for dilution.

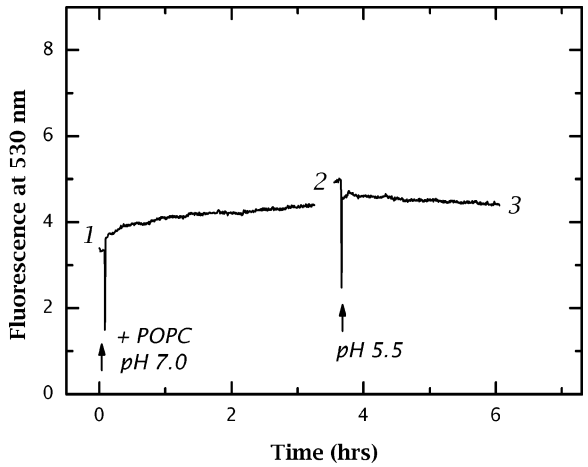

FIGURE 3: Membrane interactions of DTT with LUV formed from neutral (zwitterionic) POPC. The fluorescence kinetics of NBD-labeled DTT L350C mutant was measured in buffer and in the presence of membranes under changing conditions of pH. Experimental conditions correspond to those described in the legend for Figure 2. While DTT shows membrane binding at neutral pH (increase of intensity from 1 to 2), the acidification of the sample did not lead to a further increase in fluorescence intensity (level 3). This contrasts strongly with the substantial increase in intensity observed with anionic membranes (compare to Figure 2).

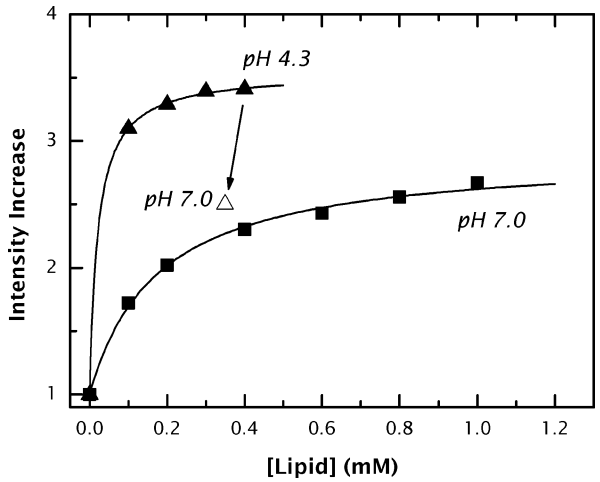

FIGURE 4: Determination of the free energy of binding of the NBD-labeled DTT Q369C mutant to 1:3 POPC/POPG LUV by means of fluorescence titration. The increase in fluorescence intensity at 530 nm is plotted against the concentration of LUV. Titration data, measured at pH 4.3 (▲) and 7.0 (■), are fitted to eq 1 (solid lines) to obtain mole-fraction partition coefficients for the calculation of free energies of transfer using eq 2 (Table 1).

relatively high pH of 7. Lowering the pH, by addition of concentrated monobasic phosphate, resulted in a further intensity increase and a further spectral shift to 528 nm (level 3). Importantly, the latter changes could be reversed by addition of concentrated dibasic phosphate, which returned the sample to pH 7 (level 4). After appropriate correction for dilution effects, the spectrum of DTT seen after reversing the pH to 7 practically coincided with the one for initial binding to LUV (spectra 2 and 4, Figure 2B). This reversible pH-triggered insertion of DTT was important, because it meant that the processes of Figure 2 were amenable to thermodynamic analysis.

We repeated the above experiments using neutral LUV made entirely from zwitterionic POPC (Figure 3) to examine the role of negatively charged lipid in the process of DTT insertion. We found that DTT will bind at neutral pH to zwitterionic membranes, resulting in the intensity of NBD fluorescence shown in the left curve of Figure 3. Importantly, the initial kinetics of membrane binding are very close to those observed for anionic membranes (Figure 2). Although the intensity did not reach equilibrium for many hours (not shown), the total intensity increase was even somewhat higher with anionic LUV (compare levels 2, Figures 2A and 3). When the pH was lowered to 5.5, the characteristic strong increase observed with anionic membranes was not seen (compare levels 3, Figures 2A and 3). We concluded that DTT can bind to zwitterionic vesicles at neutral pH but cannot refold at acid pH in a manner that causes an increase in fluorescence.

To estimate the free energy of transfer of DTT into anionic lipid membranes, we titrated the labeled mutants with vesicles and measured the resulting increases in NBD emission intensity. The results of the fluorescence titration of DTT369-NBD with LUV containing 75% POPC and 25% POPG are presented in Figure 4. The fluorescence increase observed at pH 4.3 (solid triangles) was higher than that at pH 7.0 (solid squares). Following lipid titration of a sample at pH 4.3, 0.1 mL of a concentrated solution of dibasic phosphate was added to bring the pH to 7. This led to a decrease in the level of the fluorescence to a value close to the level observed for the pH 7 titration (Figure 4, open triangle). The reversibility appears to be less perfect than that seen in Figure 2 for two reasons. First, raising the pH to 7 from 4.3 requires addition of a higher concentration of phosphate salts than that from pH 5.5. Second, the comparison was made between two different samples. The difference, however, is within the range of reproducibility for even identical multiple samples. Thus, the insertion of DTT369-NBD (Figure 4) could also be reversed by increasing the pH, as with DTT350-NBD (Figure 2).

The titration data shown in Figure 4 were fitted to eq 1 by means of a least-squares minimization procedure to obtain the mole-fraction partition coefficients, K_x, and the maximal intensity increases, I_∞. The fitted solid curves in Figure 4 have the following parameter values: $K_x = (3.2 \pm 0.3) \times 10^5$ and $I_\infty = 2.90 \pm 0.04$ at pH 7, and $K_x = (2.6 \pm 0.1) \times 10^6$ and $I_\infty = 3.54 \pm 0.03$ at pH 4.3. Note that fluorescence increases to a higher level at lower pH, which is consistent with deeper insertion into the bilayer. This pH-dependent difference was also observed for DTT350-NBD but not for DTT380-NBD (data not shown), which has a probe attached to a site not expected to insert (*7*, *8*, *25*).

The free energies of transfer of DTT from the aqueous environment to the lipid bilayer, calculated from the values of mole-fraction partition coefficients using eq 2, are summarized in Table 1. Membrane binding of the DTT350-NBD mutant at pH 4.3 was found to be so tight that we saw no change in fluorescence after 0.05 mM of lipid was added. To go below this concentration required that the protein concentration be reduced as well to maintain the dilute regime. This, in turn, reduced the reliability of the measurements and placed an ultimate upper limit on the value of ΔG that could be determined experimentally (*29*). We estimate that the limiting value is about -10 kcal mol^{-1} (Table 1). At neutral pH, the increase in fluorescence of DTT350-NBD upon binding to membranes was much

Table 1: Experimentally Determined Free Energies (kcal mol^{-1}) of Membrane Partitioning of NBD-Labeled DTT Mutants Determined by Spectroscopic Titration Measurements Such as Those of Figure 4[a]

	pH 7.0	pH 4.3
DTT350-NBD	*b*	< -10[c]
DTT369-NBD	-7.5 ± 0.3	-8.7 ± 0.5
DTT380-NBD	-7.3 ± 0.4	-7.8 ± 0.4

[a] The means and standard deviations are derived from triplicate measurements. [b] Binding at neutral pH could not be quantitated because of the small fluorescence increase (see Figure 2). [c] Binding of this mutant at low pH is too strong to be accurately determined by the spectroscopic method employed (see text).

smaller than that at pH 4.3 (Figure 2), which prevented accurate determination of ΔG. The possible origins of the variation in the ΔG values among the mutants are discussed below. Despite the differences, all mutants have important similarities: They all appear to bind to membranes at neutral pH and reversibly insert upon lowering the pH in the presence of anionic lipids. Interestingly, although each mutant has a somewhat more favorable interaction energy at low pH (Table 1), the effect of pH on binding is rather modest.

Hydropathy Analysis for DTT Transfer to Interfacial and Transmembrane States. We used a novel Java-based web tool, MPEx (http://blanco.biomol.uci.edu/mpex), to analyze DTT hydropathy plots at low and neutral pH. MPEx was well suited to the analysis for two reasons. First, the program utilizes the Wimley−White experiment-based hydrophobicity scales, which permit analysis of both the interfacial and transmembrane propensities of amino acid sequences (*22*). Second, both the interface (*15*) and transmembrane (*23*) scales include free energy values for the charged and neutral forms of aspartate, glutamate, and histidine. The results are presented in Figure 5. The upper and lower pairs of plots are for transmembrane (TM) and interfacial interactions, respectively. The left and right plots for each pair are for interactions at neutral and acid pH values, respectively.

The upper panels (panel A) of Figure 5 are for TM helices and the lower panels (panel B) for interfacial association of unfolded segments with zwitterionic membranes. The purple bars in both panels signify the helical regions of the crystallographic structure of DTT (Figure 1A). The red HΦ plot in Figure 5A and the blue HΦ plot in Figure 5B, corresponding, respectively, to the transmembrane (octanol) and interfacial scales, use a 19-residue sliding-window sum. As described in Materials and Methods, each point of a plot that has a positive value corresponds to a favorable free energy of association with the membrane. The sequence regions favoring HΦ membrane association are indicated in panels A and B by horizontal red and blue bars, respectively. The octanol (TM) scale (*24*) accurately estimates the energetics of transferring a folded helix between membrane and water (*23*), whereas the interfacial scale (*15*) accurately estimates the energetics of transferring an unfolded peptide chain between water and the interfacial region of a neutral lipid bilayer (*12*). The interfacial scale accounts for neither free energy gains upon formation of an α-helix on membrane interfaces (estimated (*30*) to be 0.4 kcal mol^{-1} per residue) nor free energy changes associated with charge−charge interactions between the protein and the membrane (*12*). To quantitate the latter contributions, we estimated the electrostatic free energy component as described in Materials and Methods. The green trace in panel B represents the sum of this ES component and the HΦ component (blue trace).

The left- and right-hand plots in each panel allow the effects of changes in the protonation states of aspartate, glutamate, and histidine residues to be assessed upon changing the pH from neutral to acid values. The left-hand plots are thus for His^0 and Asp^- and Glu^-, and the right-hand plots for His^+ and Asp^0 and Glu^0. For all plots for both scales, substantial portions of the hydropathy traces are found above the zero level in all cases, suggesting favorable membrane interactions (marked by the red, blue, and green bars above the plot).

The proposed topology for the so-called open channel state based upon direct experiments (*9*) suggests that helices TH5, TH8, and TH9 span the membrane, consistent with our hydropathy analysis. What is surprising, at least at first glance, is that practically the same TM regions are also predicted at neutral pH. Yet none of the literature on diphtheria toxin suggests membrane insertion or translocation at neutral pH. Thus, hydropathy analyses that consider only two states, TM and aqueous, are not capable of explaining the pH-dependent insertion of DTT. A control mechanism for pH-dependent insertion is suggested by the interfacial hydropathy analyses (Figure 5B), which show that interfacial partitioning depends strongly on pH. At neutral pH (left-hand plot), the TH5, TH8, and TH9 segments are predicted to interact favorably, though marginally, with the interfacial region. At low pH (right-hand plot), on the other hand, the favorable region for interfacial interactions covers almost the entire protein (green bar, right-hand plot), especially when favorable charge interactions are taken into account (green curves). This analysis suggests that at low pH, where histidine is positively charged and aspartate and glutamate are neutral, there is a dramatic increase in the interfacial association of the protein with the membrane interface. This increased interfacial association implies that DTT refolds into an interfacial intermediate state that is subsequently converted into the final transmembrane state.

DISCUSSION

The most important result of this study is that we have established the reversibility of pH-triggered membrane insertion of DTT (Figure 2), which allows us to take the first steps in experimental characterization of the thermodynamics of the refolding/insertion process (Figure 4, Table 1). Understanding the energetics of establishing a transmembrane structure is an essential step in deciphering the membrane protein folding problem.

How, exactly, can a transmembrane helical structure be established? It can occur either cotranslationally with the help of a translocon machinery (*31*) as in the case of constitutive proteins or spontaneously, as in the case of nonconstitutive proteins, such as DTT. Despite the obvious mechanistic differences between the pathways, in both cases the polypeptide chain must overcome certain energetic barriers on the way to its final lowest free energy state in the membrane. Hydropathy plots, such as those in Figure 5, allow one to locate likely transmembrane segments from the sequence (*23*). We are a long way, however, from being able to predict the tertiary structure and stability of membrane proteins. One

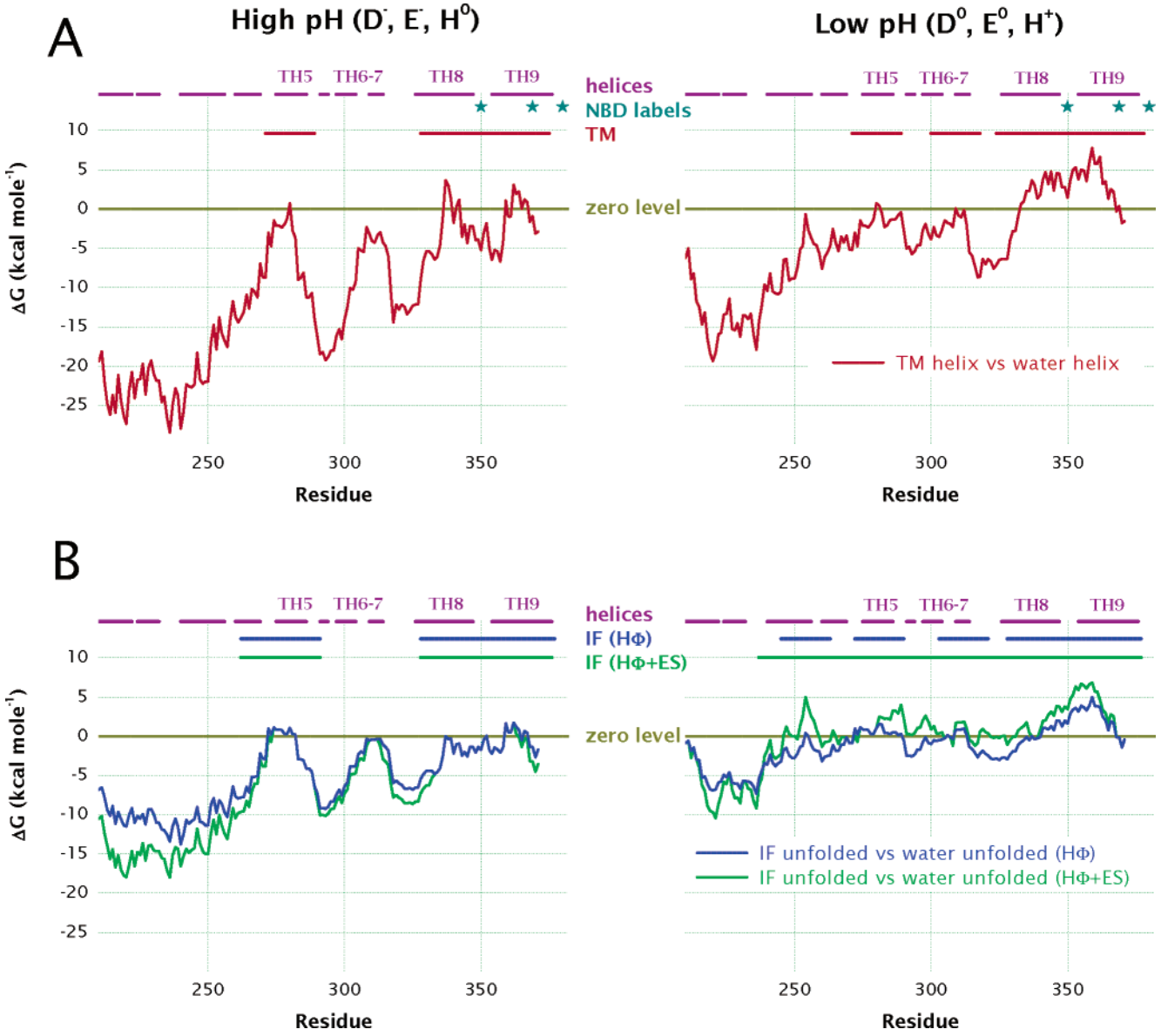

FIGURE 5: Hydropathy analysis of membrane interactions of diphtheria toxin T-domain (see text). All hydropathy plots represent a 19-residue sliding-window sum of residue free energies implemented using Membrane Protein Explorer (MPEx), which is available over the World Wide Web from the University of California at Irvine as a Java applet (http://blanco.biomol.uci.edu/mpex). The zero level distinguishes favorable from unfavorable interactions (see text). The default implementation of MPEx provides estimates of free energies of transfer from membrane to water. Consequently, any positive HΦ plot point level represents a favorable transfer free energy for the entire 19-residue sequence centered at this point. The purple bars indicate the locations of helices observed in the crystal structure of the soluble DTT (Figure 1A). Stars mark the positions where single-cysteine mutants were labeled with NBD. Left-hand plots correspond to the high-pH state and the right-hand plots to the low-pH state (see text). Panel A shows the hydropathy plots (red curves) analyzing TM helix insertion using the Wimley−White octanol scale (*23*, *24*). The red horizontal bars indicate the regions of favorable interactions. Notice that the regions for favorable TM insertion do not depend strongly on pH. Panel B shows the hydropathy plots (blue curves) analyzing favorable interfacial associations with zwitterionic membranes using the Wimley−White interfacial hydrophobicity scale (*15*, *22*). Notice that regions of interfacial association depend strongly on pH. The associations are even stronger when electrostatic interactions are taken into account (green curves). The green curves represent the sums of hydrophobic (HΦ, blue traces) and Coulombic electrostatic (ES) free energies arising from interactions between the charged protein residues and anionic lipids. The latter components were estimated by assuming a membrane surface potential of −40 mV, which corresponds to our experimental conditions. Blue (HΦ only) and green bars (HΦ + ES) represent regions with favorable interfacial transfer free energies of the unfolded chain relative to water.

of the principal difficulties is the severe shortage of direct experimental data on the stability of membrane proteins. This shortage is due in large measure to the fact that many direct experimental approaches successfully used in soluble protein studies, for example, thermal and chemical denaturation, are inapplicable to membrane proteins. To overcome this difficulty, we have devised an approach that allows useful thermodynamic information to be extracted from data on membrane partitioning of short soluble peptides (*21*, *32*). The present work is a logical extension of this approach to the more complex and challenging task of determining experimentally the free energy of membrane interaction of a self-inserting membrane protein, DTT.

We used the three single-cysteine mutants of DTT, labeled with NBD fluorescent dye, to study protein interactions with neutral and charged lipid membranes (LUV). The probes were placed in and around the consensus insertion helix TH9 (*7*, *25*) in such a way that they were exposed to the solvent

at three different sites of the folded protein (Figure 1). The use of the very bright NBD dye has a major advantage over tryptophan (*33*), which is traditionally used in membrane titration experiments (*34*, *35*). By placing the probes on the solvent-accessible sites, we were able to increase the sensitivity for detecting initial membrane binding events, which would not necessarily cause measurable changes in the environment of tryptophan residues buried within DTT. The similarity in the interaction patterns observed for all three mutants indicates an underlying common behavior of DTT and argues against substantial perturbations caused by labeling.

At pH 7, where DTT is believed to be in a fully folded membrane-incompetent state, we observed interactions with both anionic and zwitterionic LUV (Figures 2 and 3, respectively). When the pH was lowered, two of three mutants exhibited substantial increases in fluorescence, consistent with transmembrane insertion. As expected, the DTT380-NBD mutant did not show this increase, because the probe was located at the very far end of TH9, which is not expected to insert in the membrane at low pH (*7*, *25*). The insertion of the other two sites, residues 350 and 369, required the presence of anionic lipids, which is a common requirement for spontaneously inserting proteins (*11*, *35*, *36*). Although electrostatic interactions no doubt aid targeting to the membrane interface, our results suggest that they are not essential for initial binding. Rather, they may be more important for refolding on the membrane interface to set up the membrane/protein system for transmembrane insertion and translocation. This speculation is strongly supported by our hydropathy calculations (Figure 5). The fine interplay of HΦ and ES interactions has been suggested to influence the proper membrane insertion of many membrane-active proteins and peptides (*11*, *12*, *33*, *36*, *37*).

The reversible nature of membrane interaction allows one to explore the energetics of the refolding/insertion process, as we have begun to do in this study using fluorescence titration methods (Figure 4, Table 1). The partitioning free energies of Table 1 are not inconsistent with the interaction free energies implied by the hydropathy analysis (Figure 5). It is interesting that the average free energy of transfer (Table 1), -7.8 ± 0.6 kcal mol^{-1}, is about the same as the value of -7.6 kcal mol^{-1} observed for the simple membrane-active peptide melittin (*30*). All mutants have somewhat stronger membrane affinities at low pH than at neutral pH, but the differences are surprisingly small. The DTT350-NBD has the highest partitioning free energy at low pH, while the DTT380-NBD has the lowest. The difference of over 2 kcal mol^{-1} is significant and might be related to several possible causes, including some destabilization of the folded DTT by labeling (in the case of DTT350-NBD) or local flexibility that allows the site to leave the membrane temporarily, even though much of the rest of the protein is still associated with it (DTT380-NBD).

Molten globule intermediate states have been proposed to play a special role during membrane insertion and translocation (*5*, *38*−*40*). The proposed mechanism considers the formation of the molten globule near the membrane surface and attributes it to variation in local and bulk pH. This could be followed by the formation of refolded intermediate submerged into the thick interfacial region of the bilayer (*41*), a region suggested to play an important role in protein refolding (*32*). This intermediate is expected to be rich in secondary structure but lacking the specific tertiary contacts of either the initial water-soluble state or the final fully inserted state. Indeed, such intermediates were identified for the colicin E1 channel-forming domain (*13*, *14*) and annexin 12 (*33*). We do not know at the moment whether membrane-bound DTT at high pH is such an intermediate or whether it preserves some of its original tertiary fold.

The efficiency of the final insertion from the membrane interface will depend on the free energy difference between the transmembrane and interfacial conformations. The direct comparison between the corresponding traces in Figure 5 is complicated by the difference in the folding state (helical for upper panel and unfolded for the lower one). Because DTT is folded in solution, the gain in free energy due to interfacial folding (*30*) will be offset by the penalty due to unfolding in solution. These thermodynamic considerations by no means suggest that DTT has to unfold to random coil, bind, and then gain back helicity. This is most certainly not the case, and our analysis of different components of free energy follows the *thermodynamic cycle*, not the *insertion pathway*.

Another energetic component missing from our analysis (and for that matter from any hydropathy analysis) concerns contribution associated with changes in the tertiary structure of the soluble protein or its state of aggregation. Thus, the large free energy value predicted for the transition between the unfolded peptide chain in water and the helical interfacial state does not immediately imply that the *folded* state of DTT should associate with the membrane with high free energy. This transition will be opposed by the free energy of folding in solution. As a result, the transitions between states I and IV, and II and III (Figure 1) will be affected by the relative stability of membrane-associated and soluble structures at either pH.

The work presented here emphasizes the importance of the interfacial state, which should be considered explicitly in predicting membrane association of nonconstitutive proteins, such as bacterial toxins, colicins, or annexins. There is no reason to believe that interfacial interactions are important only for nonconstitutive membrane proteins. One can reasonably speculate that they may also be important in the assembly of constitutive membrane proteins. Certainly we are at the very beginning of experimental exploration of the stability of membrane proteins. However, the important fact of reversibility of membrane insertion, reported here with DTT, is an important first step toward achieving this goal.

ACKNOWLEDGMENT

We are grateful to Mr. Michael Myers for his editorial assistance.

REFERENCES

1. Pfanner, N., and Truscott, K. N. (2002) Powering mitochondrial protein import, *Nat. Struct. Biol. 9*, 234−236.
2. Takaoka, Y., Pasenkiewicz-Gierula, M., Miyagawa, H., Kitamura, K., Tamura, Y., and Kusumi, A. (2000) Molecular dynamics generation of nonarbitrary membrane models reveals lipid orientational correlations, *Biophys. J. 79*, 3118−3138.
3. Johnson, A. E., and Haigh, N. G. (2000) The ER translocon and retrotranslocation: Is the shift into reverse manual or automatic? *Cell 102*, 709−712.

4. Oh, K. J., Senzel, L., Collier, R. J., and Finkelstein, A. (1999) Translocation of the catalytic domain of diphtheria toxin across planar phospholipid bilayers by its own T domain, *Proc. Natl. Acad. Sci. U.S.A. 96*, 8467−8470.
5. Ren, J., Kachel, K., Kim, H., Malenbaum, S. E., Collier, R. J., and London, E. (1999) Interaction of diphtheria toxin T domain with molten globule-like proteins and its implications for translocation, *Science 284*, 955−957.
6. Weiss, M. S., Blanke, S. R., Collier, R. J., and Eisenberg, D. (1995) Structure of the isolated catalytic domain of diphtheria toxin, *Biochemistry 34*, 773−781.
7. Oh, K. J., Zhan, H., Cui, C., Hideg, K., Collier, R. J., and Hubbell, W. L. (1996) Organization of diphtheria toxin T domain in bilayers: A site-directed spin labeling study, *Science 273*, 810−812.
8. Oh, K. J., Zhan, H., Cui, C., Altenbach, C., Hubbell, W. L., and Collier, R. J. (1999) Conformation of the diphtheria toxin T domain in membranes: A site-directed spin-labeling study of the TH8 helix and TL5 loop, *Biochemistry 38*, 10336−10343.
9. Senzel, L., Gordon, M., Blaustein, R. O., Oh, K. J., Collier, R. J., and Finkelstein, A. (2000) Topography of diphtheria toxin's T domain in the open channel state, *J. Gen. Physiol. 115*, 421−434.
10. Wang, Y., Malenbaum, S. E., Kachel, K., Zhan, H. J., Collier, R. J., and London, E. (1997) Identification of shallow and deep membrane-penetrating forms of diphtheria toxin T domain that are regulated by protein concentration and bilayer width, *J. Biol. Chem. 272*, 25091−25098.
11. Chenal, A., Savarin, P., Nizard, P., Guillain, F., Gillet, D., and Forge, V. (2002) Membrane protein insertion regulated by bringing electrostatic and hydrophobic interactions into play. A case study with the translocation domain of the diphtheria toxin, *J. Biol. Chem. 277*, 43425−43432.
12. Ladokhin, A. S., and White, S. H. (2001) Protein chemistry at membrane interfaces: Non-additivity of electrostatic and hydrophobic interactions, *J. Mol. Biol. 309*, 543−552.
13. Zakharov, S. D., Lindberg, M., Griko, Y., Salamon, Z., Tollin, G., Prendergast, F. G., and Cramer, W. A. (1998) Membrane-bound state of the colicin E1 channel domain as an extended two-dimensional helical array, *Proc. Natl. Acad. Sci. U.S.A. 95*, 4282−4287.
14. Zakharov, S. D., Lindeberg, M., and Cramer, W. A. (1999) Kinetic description of structural changes linked to membrane import of the colicin E1 channel protein, *Biochemistry 38*, 11325−11332.
15. Wimley, W. C., and White, S. H. (1996) Experimentally determined hydrophobicity scale for proteins at membrane interfaces, *Nat. Struct. Biol. 3*, 842−848.
16. Zhan, H., Elliott, J. L., Shen, W. H., Huynh, P. D., Finkelstein, A., and Collier, R. J. (1999) Effects of mutations in proline 345 on insertion of diptheria toxin into model membranes, *J. Membr. Biol. 167*, 173−181.
17. Haugland, R. P. (1996) *Handbook of Fluorescent Probes and Research Chemicals*, Molecular Probes, Inc., Eugene, OR.
18. Mayer, L. D., Hope, M. J., and Cullis, P. R. (1986) Vesicles of variable sizes produced by a rapid extrusion procedure, *Biochim. Biophys. Acta 858*, 161−168.
19. Hope, M. J., Bally, M. B., Mayer, L. D., Janoff, A. S., and Cullis, P. R. (1986) Generation of multilamellar and unilamellar phospholipid vesicles, *Chem. Phys. Lipids 40*, 89−107.
20. Ladokhin, A. S., Jayasinghe, S., and White, S. H. (2000) How to measure and analyze tryptophan fluorescence in membranes properly, and why bother? *Anal. Biochem. 285*, 235−245.
21. White, S. H., Wimley, W. C., Ladokhin, A. S., and Hristova, K. (1998) Protein folding in membranes: Determining the energetics of peptide-bilayer interactions, *Methods Enzymol. 295*, 62−87.
22. White, S. H., and Wimley, W. C. (1999) Membrane protein folding and stability: Physical principles, *Annu. Rev. Biophys. Biomol. Struct. 28*, 319−365.
23. Jayasinghe, S., Hristova, K., and White, S. H. (2001) Energetics, stability, and prediction of transmembrane helices, *J. Mol. Biol. 312*, 927−934.
24. Wimley, W. C., Creamer, T. P., and White, S. H. (1996) Solvation energies of amino acid sidechains and backbone in a family of host−guest pentapeptides, *Biochemistry 35*, 5109−5124.
25. Kachel, K., Ren, J. H., Collier, R. J., and London, E. (1998) Identifying transmembrane states and defining the membrane insertion boundaries of hydrophobic helices in membrane-inserted diphtheria toxin T domain, *J. Biol. Chem. 273*, 22950−22956.
26. O'Keefe, D. O., Cabiaux, V., Choe, S., Eisenberg, D., and Collier, R. J. (1992) pH-Dependent Insertion of Proteins into Membranes - B- Chain Mutation of Diphtheria Toxin That Inhibits Membrane Translocation, Glu-349→Lys, *Proc. Natl. Acad. Sci. U.S.A. 89*, 6202−6206.
27. Mindell, J. A., Silverman, J. A., Collier, R. J., and Finkelstein, A. (1994) Structure function relationships in diphtheria toxin channels. II. A residue responsible for the channel's dependence on *Trans* pH, *J. Membr. Biol. 137*, 29−44.
28. Mindell, J. A., Silverman, J. A., Collier, R. J., and Finkelstein, A. (1994) Structure−function relationships in diphtheria toxin channels. III. Residues which affect the *Cis* pH dependence of channel conductance, *J. Membr. Biol. 137*, 45−57.
29. Ladokhin, A. S., Selsted, M. E., and White, S. H. (1997) Bilayer interactions of indolicidin, a small antimicrobial peptide rich in tryptophan, proline, and basic amino acids, *Biophys. J. 72*, 794−805.
30. Ladokhin, A. S., and White, S. H. (1999) Folding of amphipathic α-helices on membranes: Energetics of helix formation by melittin, *J. Mol. Biol. 285*, 1363−1369.
31. Johnson, A. E., and van Waes, M. A. (1999) The translocon: A dynamic gateway at the ER membrane, *Annu. Rev. Cell Dev. Biol. 15*, 799−842.
32. White, S. H., Ladokhin, A. S., Jayasinghe, S., and Hristova, K. (2001) How membranes shape protein structure, *J. Biol. Chem. 276*, 32395−32398.
33. Ladokhin, A. S., Isas, J. M., Haigler, H. T., and White, S. H. (2002) Determining the membrane topology of proteins: Insertion pathway of a transmembrane helix of annexin 12, *Biochemistry 41*, 13617−13626.
34. Wang, Y., Kachel, K., Pablo, L., and London, E. (1997) Use of Trp mutations to evaluate the conformational behavior and membrane insertion of A and B chains in whole diphtheria toxin, *Biochemistry 36*, 16300−16308.
35. Malenbaum, S. E., Collier, R. J., and London, E. (1998) Membrane topography of the T domain of diphtheria toxin probed with single tryptophan mutants, *Biochemistry 37*, 17915−17922.
36. Zakharov, S. D., Heymann, J. B., Zhang, Y.-L., and Cramer, W. A. (1996) Membrane binding of the colicin E1 channel: Activity requires an electrostatic interaction of intermediate magnitude, *Biophys. J. 70*, 2774−2783.
37. Ladokhin, A. S., and White, S. H. (2001) 'Detergent-like' permeabilization of anionic lipid vesicles by melittin, *Biochim. Biophys. Acta 1514*, 253−260.
38. Bychkova, V. E., Pain, R. H., and Ptitsyn, O. B. (1988) The "molten globule" state is involved in the translocation of proteins across membranes? *FEBS Lett. 238*, 231−234.
39. van der Goot, F. G., González-Mañas, J. M., Lakey, J. H., and Pattus, F. (1991) A molten-globule membrane-insertion intermediate of the pore-forming domain of colicin A, *Nature 354*, 408−410.
40. Bychkova, V. E., Dujsekina, A. E., Klenin, S. I., Tiktopulo, E. I., Uversky, V. N., and Ptitsyn, O. B. (1996) Molten globule-like state of cytochrome *c* under conditions simulating those near the membrane surface, *Biochemistry 35*, 6058−6063.
41. White, S. H., and Wiener, M. C. (1995) Determination of the structure of fluid lipid bilayer membranes, in *Permeability and Stability of Lipid Bilayers* (Disalvo, E. A., and Simon, S. A., Eds.) pp 1−19, CRC Press, Boca Raton, FL.
42. Wiener, M. C., and White, S. H. (1992) Structure of a fluid dioleoylphosphatidylcholine bilayer determined by joint refinement of X-ray and neutron diffraction data. III. Complete structure, *Biophys. J. 61*, 434−447.
43. White, S. H., and Wiener, M. C. (1996) The liquid-crystallographic structure of fluid lipid bilayer membranes, in *Membrane Structure and Dynamics* (Merz, K. M., and Roux, B., Eds.) pp 127−144, Birkhäuser, Boston.

BI036157W